



Research article

# Strain concentration of double-edge hole ductile composites in the full range of deformation by digital image correlation

Sanjay Kumar<sup>1</sup>, Chang-Mou Wu<sup>1\*</sup>, Po-Chun Lin<sup>1</sup>, Jieng-Chiang Chen<sup>2</sup>, Yoshinobu Shimamura<sup>3</sup>

<sup>1</sup>Department of Materials Science and Engineering, National Taiwan University of Science and Technology, No. 43, Keelung Rd., Sec.4, Da'an Dist., 10607 Taipei, Taiwan (R.O.C.)

<sup>2</sup>Department of Fashion Styling & Design, Vanung University, Chungli Dist., 320313 Taoyuan, Taiwan (R.O.C.)

<sup>3</sup>Department of Mechanical Engineering, Shizuoka University, 3-5-1 Johoku, Naka-ku, Hamamatsu, 432-8561 Shizuoka, Japan

Received 4 May 2022; accepted in revised form 11 June 2022

**Abstract.** This study investigated variations in strain concentration factors ( $K_e$ ) within the full deformation range of self-reinforced poly(ethylene terephthalate) composites (srPETs) with double-edge semicircular holes (DESH) using digital image correlation (DIC) at different width-to-diameter ( $W/D$ ) ratios. The value of  $K_e$  agrees with the theoretical concentration factor ( $K_t$ ) within the elastic deformation range; then, it increases rapidly to a peak because of plastic deformation. Therefore, the change in  $K_e$  was divided into different stages based on the spread of the yield extent (beginning from the hole edge). These results will help improve the understanding of the yielding phenomenon of open-hole materials and provide early warnings before final material damage.  $K_e$  decreased in both the elastic and plastic regions with a decrease in  $W/D$ ; however, there was an exception when the  $W/D$  ratio = 1.5. Therefore, the geometric configuration  $W/D > 1.5$  was recommended for designing secure structural ductile composites. The  $K_e$  of DESH is lower than that of circular holes (CH) in both the elastic and plastic regions for the hole effect. Thus, composites with DESH should be preferred as an alternative for structural applications.

**Keywords:** polymer composites, materials testing, mechanical properties, strain concentration, digital image correlation method

## 1. Introduction

Fiber-reinforced polymer composites (FRPCs) are well known for their excellent strength-to-weight and stiffness-to-weight ratios. FRPCs are widely used instead of conventional metal materials in various industrial and research applications because of their superior properties. Advanced technologies are being used in the manufacturing of FRPCs to fulfill the current demand for FRPCs; however, this generates a significant amount of polymer waste, which ends up as an environmental pollutant [1–4]. Thus, it is necessary to focus on reusable and recyclable materials to protect the environment.

Among various recyclable FRPCs [5–7], self-reinforced polymer composites (srPCs), which are also referred to as single polymer or all-polymer composites, are known for being easily recycled and reprocessed through melting [8–11]. Poly(ethylene terephthalate) (PET) has been one of the foremost engineering polymers in the past two decades because of its excellent performance properties and easy recyclability [12]. Therefore, PET is the most viable candidate polymer for manufacturing srPC [12–14]. The self-reinforced poly(ethylene terephthalate) (srPETs) composites were produced by film stacking from fabrics that comprise double-covered

\*Corresponding author, e-mail: [cmwu@mail.ntust.edu.tw](mailto:cmwu@mail.ntust.edu.tw)  
© BME-PT

uncommingled yarns in the author's laboratory [15]. Long-term creep behavior, open-hole tensile properties, fracture behavior, pinhole tensile, and fatigue properties of srPET composites have recently been studied [15–19]. These studies reported that srPET composites exhibit superb ductility, notch insensitivity, superior creep resistance, higher resistance to crack initiation, and better pin load behavior. Further, these studies have suggested that srPET composites can be used in a secure environment to avoid expeditious damage.

In industries where srPET composites can be applied in automobiles and industrial parts, the parts can be joined by mechanical joints; their designs often include holes to connect the structural parts. These holes present either stress or strain concentration (SC), and this consequently decreases the load-carrying capacity of composite materials. Therefore, it is necessary to observe the effect of the SC on the performance of the composites with holes.

The SC of a material depends on the hole type and size. Most studies focused on circular holes because they are used for industrial applications. Evaluation using Roark's formulas illustrates that  $K_t$  increases with an increase in  $W/D$  when axial tension is applied to a sample with a circular hole within a linear elastic state [20]. In our previous study [19], Neuber's rule was applied to observe the stress concentration factor ( $K_\sigma$ ) and strain concentration factor ( $K_\epsilon$ ). The results show that  $K_\sigma$  and  $K_\epsilon$  increase with an increase in  $W/D$ , and they agree with the evaluation performed using  $K_t$ . Researchers have attempted to mitigate SC using different techniques for increasing the life of composites. Most studies used functionally graded materials around a hole to reduce  $K_\sigma$  [21–23]. Another approach to reducing  $K_\sigma$  was plastic deformation, and it is known that the plasticity of ductile materials relieves SC. The stress distribution around the hole in plastic form is employed to transfer and cause a reduction in the SC at a structure comprising a highly ductile material [24].

Brittle materials do not have sufficient ductility; the notch effect may be an SC that leads to brittle fracture [24]. Shi and Plus [25] analyzed a series of notched components with high yield strengths. They found that  $K_\sigma$  was significantly reduced because of the formation of plastic yielding around the notch;  $K_\sigma$  decreases with an increase in load, and it is equal to  $K_t$  only if no plastic yielding occurs at the notch. Several studies on ductile materials indicated that  $K_\sigma$

mitigation can be attributed to plastic yielding [26–28]. According to the studies on elasticity and SC,  $K_\sigma$  obtained in the elastic state is equivalent to  $K_\epsilon$ , however, the values of  $K_\epsilon$  and  $K_\sigma$  are different after the elastic state because of the plastic deformation [29]. Therefore, it is necessary to study  $K_\sigma$  and  $K_\epsilon$  during plastic deformation; the plastic deformation of the ductile materials plays a crucial role in determining their life. Therefore, for ductile srPETs, yielding near the hole would allow larger plastic deformation, and this can reduce the SC and extend the load-bearing behavior of the composite.

Another approach to reducing  $K_\sigma$  involves the use of multiple holes [30, 31]; this approach reduces  $K_\sigma$  values by 10 to 20% by introducing holes on both sides [30, 32]. The stress and strength of composite laminates with two interacting holes were analyzed [33], and the maximum  $K_\sigma$  was observed in the sample with a hole orientation of 22.5°, whereas the minimum  $K_\sigma$  was observed with the hole orientation at 90°. This result indicates that  $K_\sigma$  can be minimized by the interaction between two or multiple holes. Therefore, it is crucial to observe how the strain/stress interaction or coupling of composites with multiple holes that contribute to the reduction in SC and leads to an increase in the composite lifetime. However, no studies have reported the SC of ductile composites with multiple pores. Furthermore, SC near the hole could not be obtained using a mechanical testing system (MTS).

There are several experimental methods for measuring the strain/stress [20, 34]. The strain gauges are the most widely used methods for strain measurements and stress analysis. However, strain gauges are limited in obtaining the strain/stress at a single point and in one direction; therefore, they are not suitable for strain field studies [22, 35]. Another limitation of the strain gauge is that its detection range does not allow full-scale deflection, and thus, it is unsuitable for large deforming materials [36]. The photoelastic method has been widely used to determine the full stress/strain field of composites [37–39]. Some disadvantages that limit its application are (1) the time-consuming manufacturing process of model specimens for structures with complicated shapes; (2) high residual stress contained in the photoelastic model material; and (3) secure adhesion of the photoelastic coatings to the structure to ensure proper strain transmission on the surface [40, 41].

Considering the drawbacks of the above-mentioned methods, DIC is used for its powerful ability to analyze material deformation and damage behavior [42]. And successfully observed the variations in the  $K_\varepsilon$  and  $K_\sigma$  of srPETs with circular holes [43]. In this study, the variation in  $K_\varepsilon$  with full-range deformation of srPETs with a double-edged semicircular hole was investigated using DIC. Finally, the effects of  $W/D$  on  $K_\varepsilon$  and the contribution of strain coupling to the SC reduction of srPETs were investigated.

## 2. Experimental procedure

### 2.1. Materials and specimen preparation

The materials used in this study were similar to those used in our previous study [15]. PET (rPET) yarns spun from recycled soft drink bottles were used as reinforcements. The rPET yarns consisted of 111 tex multifilament bundles exhibiting tenacity of 65.4 g/tex and, an elongation of 25.3%. Every multifilament bundle contained 192 filaments. Yarns of PET copolymer (mPET) served as matrices after hot pressing in the corresponding self-reinforced PET composites. The mPET yarns consisted of 35.6 tex multifilament bundles with a tenacity of 42.8 g/tex and elongation of 27.9%. The mPET bundles contained 96 filaments. The rPET and mPET yarns were combined in double-covered un-commingled yarns (DUCY) using a hollow spindle spinning machine. However, to obtain an even distribution of the reinforcing fibers, the fiber and matrix volume fraction was set as 53/47. This was achieved by selecting the appropriate spinning parameters. The DUCY was supplied as feed material in the fabrication of 2/2 basket-woven fabric. The warp and weft yarn densities of the 2/2 basket-woven fabric were 13.4 and 11.8 bundles/cm, respectively. The industrial-scale hot press system (FC-650TON, Long Chang, Taiwan) was used to fabricate the srPET composites into a dimension of  $1 \times 1 \text{ m}^2$  sheets. The srPET composites had a thickness of 2 mm and were prepared by using five stacking layers of basket fabric subjected to a pressure of 12 MPa at 235 °C for 1 min, followed by fast cooling. A brittle plastic, polymethyl methacrylate (PMMA), was selected for comparison with ductile srPETs. PMMA, which is a commercially available product (ACA-2H), was purchased from Wumai Corp., Taiwan.

The srPET specimens with double-edge semicircular (DESH) and circular hole (CH) and different  $W/D$  ratios (3.5, 2.5, and 1.5) were prepared. The srPET

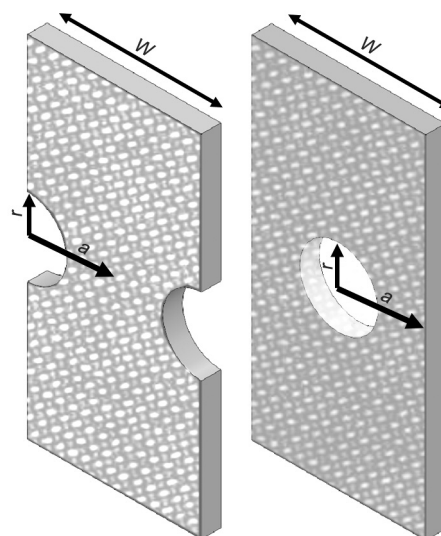


**Figure 1.** Geometric specification of srPETs with double-edge semicircular holes (DESH) and with a circular hole (CH). (Where  $r$  is the radius of the hole,  $a$  is distance on x-axis and  $W$  is the width of the specimen.)

composites with lengths and thicknesses of 200 mm and 2 mm, respectively, were used. Three different widths and a constant hole size (12 mm) were used to prepare samples with different  $W/D$  ratios. The semicircular hole was created on both sides of the edge, and a circular hole was created in the middle of the specimens. An abrasive waterjet machine (MAXIEM® 0707 Jet Machining® Center, Innovate Technologies, USA) was used for sample preparation. The water jet processing parameters are as follows: working water pressure: 350 MPa, moving speed: 200 mm/min, spacing: 1.5 mm, abrasive particle size: 80 mesh, abrasive flow: 333 g/min. Geometrical configurations of the prepared specimen are shown in Figure 1, where  $r$  represents the radius of the hole, and  $a$  represents the distance on the X-axis.

### 2.2. Experimental setup

Tensile tests were performed using a universal testing machine (MTS 810, MTS Systems Corporation, USA) with a load cell of 100 kN based on the ASTM D3039 standard. The crosshead speed was set at 5 mm/min. During the experiments, the deformation of the srPET composites with holes was evaluated using a two-dimensional (2D) DIC method. The consecutive images were captured throughout the loading period using a camera (GS3-U3-41S4C-C, Point Grey, Canada). In order to capture proper visualization of the images, white light-emitting diode (LED) lights were used to obtain appropriate lighting conditions.

The resolution of the camera is  $3 \cdot 10^{-2}$  mm/pixel, and the photographing rate is 5 frames/sec. Black paint was sprayed on the surface of the sample to obtain a random speckle pattern. Vic-2D software (Correlated Solutions, USA) was used for DIC analysis, which involved comparing images of objects before and after further deformation and presenting the acquired information in pixels. These data can be converted into the necessary metric units (strain) and formed into color contour images. Subset sizes and steps of 101 and 7 pixels were used for srPET specimens, while 55 and 7 pixels were used for brittle PMMA specimens. The Lagrangian strain tensor used to obtain strain results, it is a finite strain measurement that contain higher-order displacement terms, which describe the gradient from the original configuration. This measure is appropriate for low strains and is often used for materials subject to large strains. Therefore, it is suitable to obtain the strains of srPET and PMMA materials in this study. The Lagrangian strain equation is as Equation (1):

$$\epsilon_{yy} = \frac{dv}{dy} + \frac{\left(\frac{du}{dy}\right)^2 + \left(\frac{dv}{dy}\right)^2}{2} \quad (1)$$

where  $u$  is the X-axis displacement between the reference image and the given image, and  $v$  is the Y-axis displacement between the reference image and the given image.  $\epsilon_{yy}$  is the strain in the  $y$  direction and the term in the form of  $d$  is the gradient.

### 3. Result and discussion

#### 3.1. Tensile properties of srPETs with circular hole (CH) and double-edge semicircular hole (DESH)

The mechanical properties of srPETs with holes were dependent on the types of holes and the  $W/D$

ratios. Therefore, the net nominal stress-strain curve of srPETs with DESH was investigated, as shown in Figure 2a. They found that the net tensile strength increased, and the strain decreased with a decrease in the  $W/D$  ratio. Further, the failure strain at  $W/D$  ratio = 3.5 was 46% of the strain of the unnotched srPETs; when the  $W/D$  ratio = 1.5, the failure strain becomes 16% compared to unnotched srPETs. This is attributed to the expansion of the hole in the longitudinal direction (Figure 3) in this case ( $W/D$  ratio = 1.5) being comparatively lower than that for other  $W/D$  ratios. Therefore, it broke unexpectedly and may be attributed to higher SC, which is discussed in the next sections. The net tensile strength of srPETs with CH decreased with a decrease in the  $W/D$  ratio. However, the DESH specimens exhibited better tensile properties in terms of strength, strain, and modulus than the CH specimens.

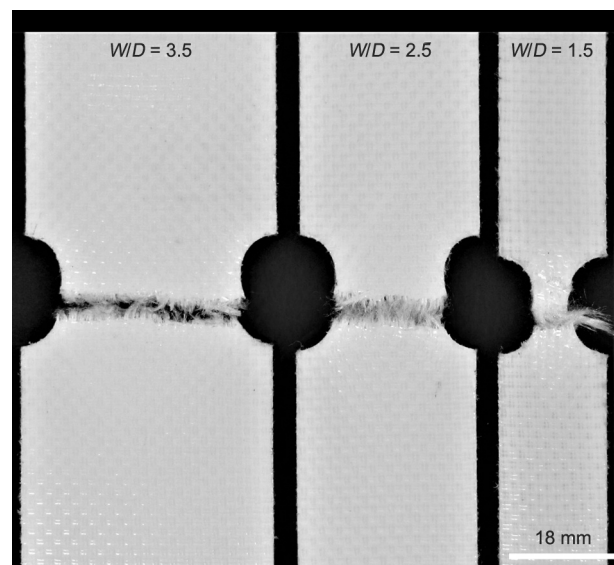


Figure 3. Fracture behavior of srPETs with DESH at  $W/D$  ratio = 3.5, 2.5, and 1.5.

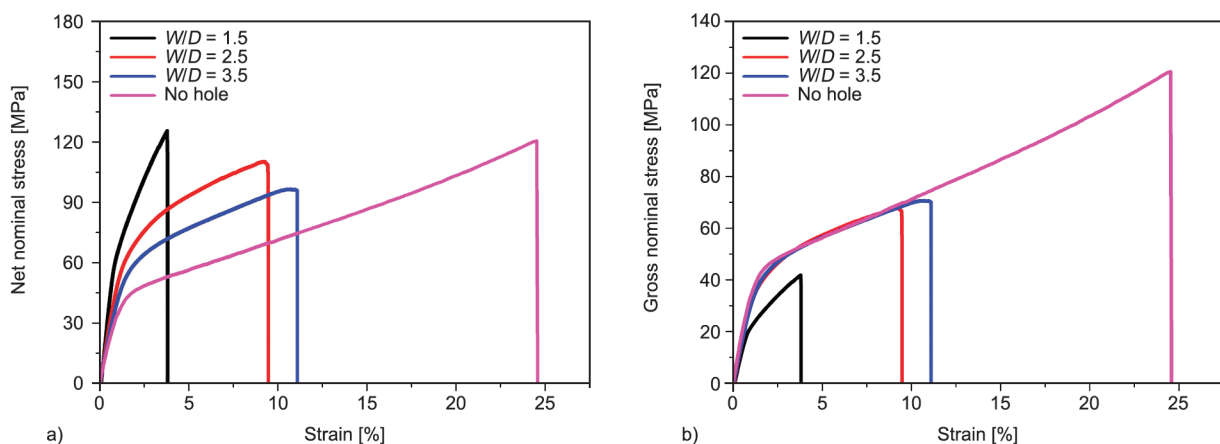


Figure 2. Stress-strain curves of srPETs with DESH. (a) Net nominal. (b) Gross nominal.



Strength retention is an important parameter in the design of engineering materials [19], and net tensile strength is a major criterion for strength retention. Thus, the strength retention of srPETs with CH and DESH has been analyzed. Several studies [44–47] have focused on carbon and glass fiber-reinforced composites that exhibit moderate strength retention (approximately 40–52%). However, in this study, the strength retention was found to be 73 and 87% for CH, and 87 and 95% for DESH at  $W/D$  ratio = 3.5 and 2.5, respectively. This indicates that srPETs have better strength retention than those of brittle composites because of their super ductile behavior. Studies on ductile composites made of kenaf or flax/polypropylene also reported similar results for strength retention behavior as srPETs, and they ranged between 84–89% at  $W/D$  ratios of 4–6 [48, 49]. However, in a study on srPP composites, the strength retention was approximately 100% at  $W/D$  ratio = 3 [50]. Further, the strength retention of srPETs with DESH was found to be equal to 100% at  $W/D$  ratio = 1.5. Such large strength retention of the composites can be attributed to the lower net nominal area of the specimens at lower  $W/D$  ratios ( $W/D \leq 2$ ). Therefore, it is necessary to observe the gross nominal behavior of the composites to determine the criterion for structural reliability. In the study of brittle carbon/ epoxy and E-glass/epoxy composites, the gross strength retention decreased from 60 to 44% and 55 to 36% as the  $W/D$  ratio decreased from 4 to 1.8 and from 3.5 to 2, respectively [47, 51]. Further, notched plates with lower  $W/D$  ratios ( $W/D$  ratio  $\leq 2$ ) are more vulnerable to damage. For ductile kenaf/polypropylene composites, the gross strength decreased from 49 to 36% as the  $W/D$  decreased from 3 to 2 [48]. These results indicate that the gross strength decreased abruptly as the  $W/D$  ratio reached  $W/D \leq 2$ . The ligament is too small to carry the load at lower  $W/D$  ratios ( $W/D \leq 2$ ), and therefore, cracks initiate earlier and propagate directly to cause the final failure. In this study, the gross strength of srPETs with DESH is analyzed, as shown in Figure 2b. The gross strength retention of srPETs decreased from 60 to 35% as  $W/D$  decreased from 3.5 to 1.5. The gross nominal stress-strain curve at  $W/D$  ratio = 1.5 does not follow that of the unnotched srPETs and deviates at 0.73% of the strain (Figure 2b). Therefore, the  $W/D$  of srPET composites at lower ratios (1.5) is not recommended for structural reliability because it is not suitable for load control and displacement control applications.

### 3.2. Strain concentration factor of PMMA with CH and DESH

The  $K_\epsilon$  values of PMMA with CH and DESH were obtained by DIC and compared with  $K_t$  (Table 1) to perceive the benefit of srPET's super ductility on  $K_\epsilon$  and reconfirm the accuracy of the DIC method. The equation for CH is reported in our previous study [19].  $K_t$  was calculated theoretically for DESH using Equation (2) [52]:

$$K_t = 3.065 - 3.472\left(\frac{2r}{W}\right) + 1.009\left(\frac{2r}{W}\right)^2 - 0.405\left(\frac{2r}{W}\right)^3 \quad (2)$$

The results show that  $K_\epsilon$  obtained by DIC is equal to  $K_t$  at  $W/D$  ratio = 3.5 and 2.5 (as indicated in Table 1). This is consistent with our previous findings that  $K_\epsilon$  should be constant and equal to  $K_o$  and  $K_t$  if the material deforms elastically [43]. Further, this finding proves that DIC is an accurate method for studying the  $K_\epsilon$  of srPETs with DESH and CH. However, there is little variation at  $W/D$  ratio = 1.5 in the DESH and CH specimens; this can be because of the effect of the smaller ligament width. In addition,  $K_\epsilon$  decreased as the  $W/D$  ratio decreased from 3.5 to 1.5 in both samples (as listed in Table 1). The  $K_\epsilon$  value of PMMA with DESH was smaller than that of PMMA with CH.

### 3.3. Strain concentration factor of srPETs with CH and DESH

The  $K_\epsilon$  values of srPET with CH and DESH for different  $W/D$  ratios are shown in Figure 4.  $K_\epsilon$  was divided into five and six stages based on the propagation of the yield extent (beginning from the hole edge) of srPETs with CH and DESH, respectively. The yield point is defined as the point on the engineering stress-strain curve that denotes the beginning of plastic deformation. However, for highly ductile materials, there is a gradual onset of nonlinear

**Table 1.** Strain concentration factor ( $K_\epsilon$ ) and theoretical stress concentration factor ( $K_t$ ) of PMMA with circular hole (CH) and double-edge semicircular hole (DESH) at different  $W/D$  ratios.

		$W/D$ [–]		
		3.5	2.5	1.5
CH	$K_t$ [–]	2.37	2.23	2.08
	$K_\epsilon$ [DIC]	2.38±0.02	2.24±0.03	2.15±0.04
DESH	$K_t$ [–]	2.16	1.86	1.29
	$K_\epsilon$ [DIC]	2.18±0.03	1.89±0.04	1.79±0.05

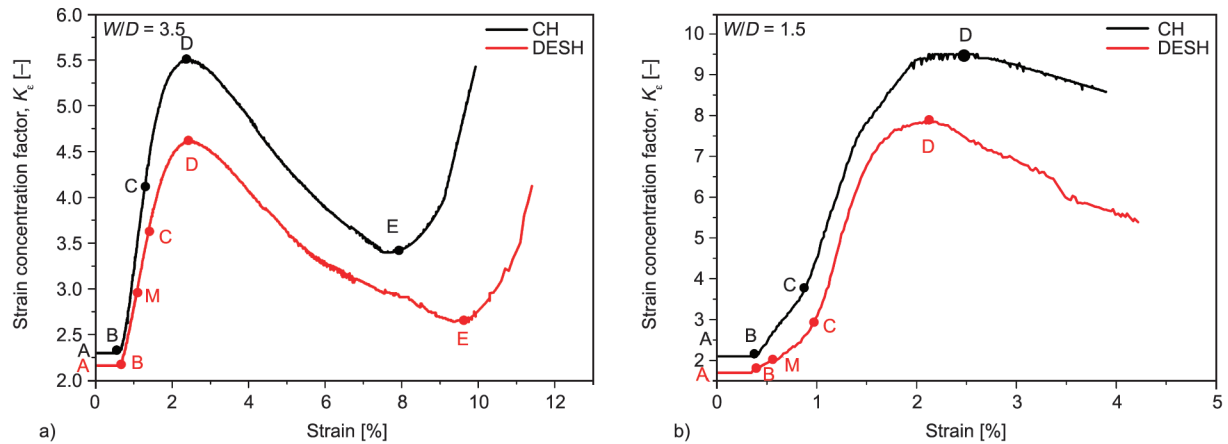


**Figure 4.**  $K_\epsilon$  of srPETs with a circular hole (CH) and double-edge semicircular hole (DESH) using the DIC method. (a) at  $W/D$  ratio = 3.5, (b) at  $W/D$  ratio = 1.5.

behavior (as indicated in Figure 2). Therefore, the offset yield point at 0.2% deformation of the specimens was considered the yield stress and yield strain ( $\epsilon_y$ ) of the specimens. Further, the  $\epsilon_y$  of the specimens was used as the maximum value of the scale in the DIC to obtain colorized strain contours at different deformation stages of the specimens (Figures 5 and 6), which clearly recognized the propagation of the yielding extent (beginning from the hole edge).

Figure 4a shows the variation in the  $K_\epsilon$  for srPETs at  $W/D$  ratio = 3.5. In stages A–B, the value of  $K_\epsilon$  of srPETs with CH is constant and equal to  $K_t$  at 2.37, which agrees with the results obtained from PMMA; this is attributed to the elastic deformation of srPETs. However, at B, the local strain at the hole edge ( $\epsilon_{\text{hole}}$ ) is equal to the yield strain ( $\epsilon_y$ ) ( $\epsilon_{\text{hole}} = \epsilon_y = 1.33\%$ , as indicated in Table 2), which implies that local yielding is triggered. In addition, this can be confirmed by the colorized strain contour (marked at the hole edge in Figure 5a). At point B, the edge of the hole becomes red, which accounts for local yielding at the hole edge.

Further deformation after point B causes the yield to propagate from the hole edge. That is, more portions of the specimen yielded with plastic deformation with an increase in the load. Further,  $K_\epsilon$  increased rapidly (Figure 4a) from B to C. At point C,  $K_\epsilon$  was 4.09, and this agrees with  $K_\epsilon$  calculated using Neuber's rule [52]. At point C, the average strain ( $\epsilon_{\text{avg}}$ ) of the specimen is equal to  $\epsilon_y$  ( $\epsilon_{\text{avg}} = \epsilon_y = 1.33\%$ , as listed in Table 2); this indicates that the yield of the specimen attributed to the local SC caused by the hole can be determined by the average strain of the specimen. The colorized contour at point C (Figure 5a) suggests that the propagation of the yield extent

reaches the edge of the specimen, which indicates that the whole ligament yielded.

During stages C–D,  $K_\epsilon$  continues to increase until it peaks at point D ( $K_\epsilon = 5.50$ ), as shown in Figure 4a. Even if  $K_\epsilon$  reaches its maximum value, it does not cause the specimen to fail because  $K_\sigma$  has a lower value, and  $\epsilon_{\text{hole}}$  is approximately half the failure strain of srPET (Table 2). At point D, the strain at the end of the specimen ( $\epsilon_{\text{end}}$ ) is equal to  $\epsilon_y$  ( $\epsilon_{\text{end}} = \epsilon_y = 1.33\%$ ), which implies that the entire specimen yielded (*i.e.*, the total yield point) (Figure 5). In addition, the entire specimen turned red on the colored strain contour (Figure 5a), which implies the propagation of the yield extent reached the end of the specimen. After point D, the difference between  $\epsilon_{\text{avg}}$  and  $\epsilon_{\text{hole}}$  decreases because the region away from the hole leads to an increase in  $\epsilon_{\text{avg}}$  through plastic deformation. This results in a gradual decrease in  $K_\epsilon$  from point D to point E, as indicated in Figure 4a. At point E,  $\epsilon_{\text{hole}}$  approaches the failure strain of srPET ( $\sim 24\%$ ), where microcracks begin to form at the edge of the hole. The specimen continues to deform plastically and cause microcracks to propagate rapidly from the edge of the hole with an increase in the load; this results in a rapid increase in  $K_\epsilon$  until the specimen fails. Therefore, point E can be used as an early warning indicator before the catastrophic failure of the sample.

The  $K_\epsilon$  response of srPET with DESH is like that of CH (as shown in Figure 4a); however, its  $K_\epsilon$  is lower throughout the deformation process because of the strain-coupling effect of srPET with DESH. For srPET with DESH, an extra point M was found. The strain at the ‘middle’ of the two semicircular holes of the specimen ( $\epsilon_{\text{middle}}$  in Figure 5b) is equal to  $\epsilon_y$

( $\epsilon_{\text{middle}} = \epsilon_y = 1.42\%$ , see Table 2), which implies that the yield growth extends to the ‘middle’. The colored contour at point M suggested that the ‘middle’

turns to red, *i.e.*, the propagation of the yield extent coupled in this region. This results in a relatively lower  $K_e$  than CH for srPET with DESH at points C

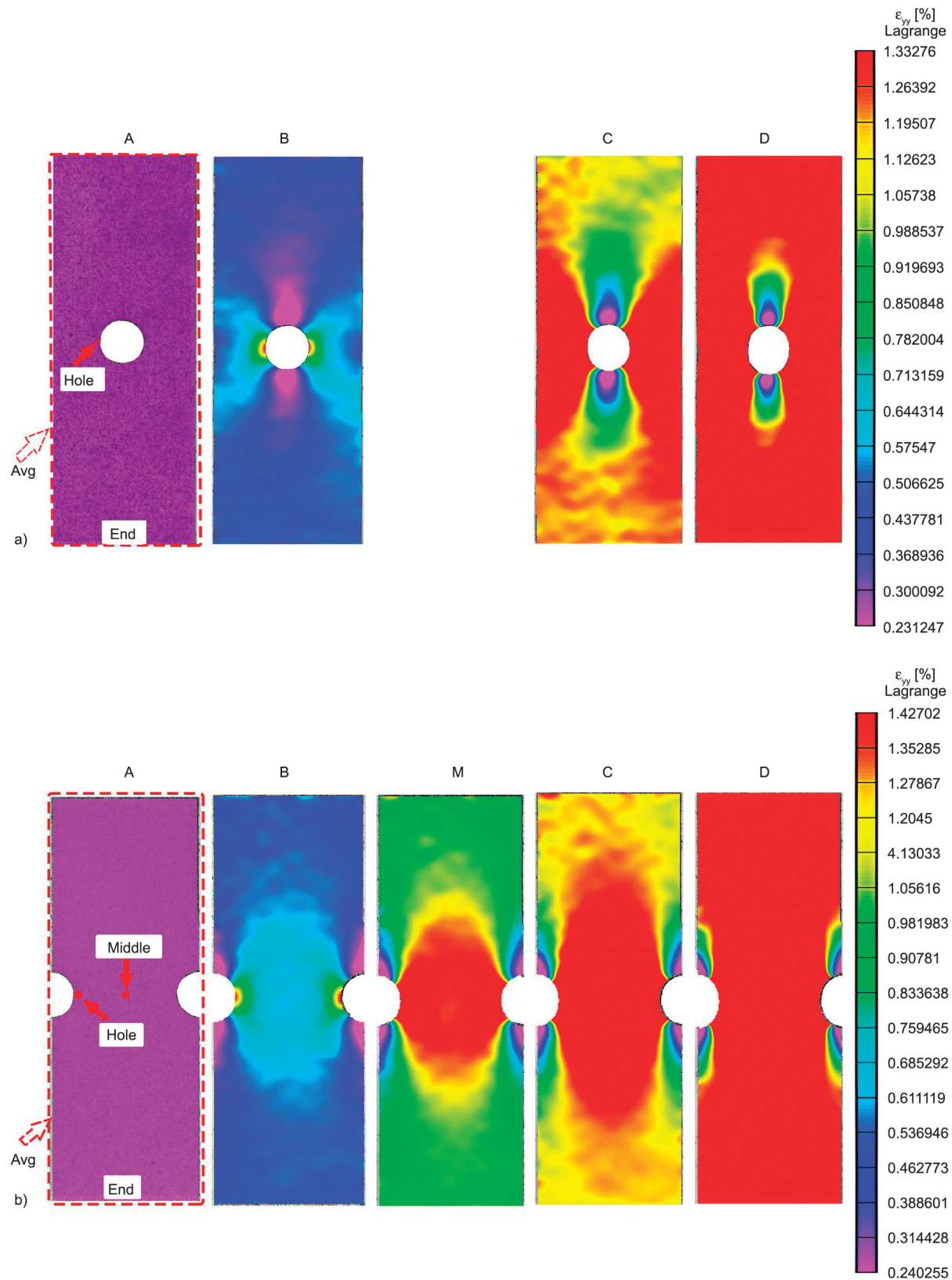


**Figure 5.** Colorized contour of srPETs at  $W/D$  ratio = 3.5. (a) Points B, C, and D for CH specimens, (b) points B, M, C, and D for DESH specimens.



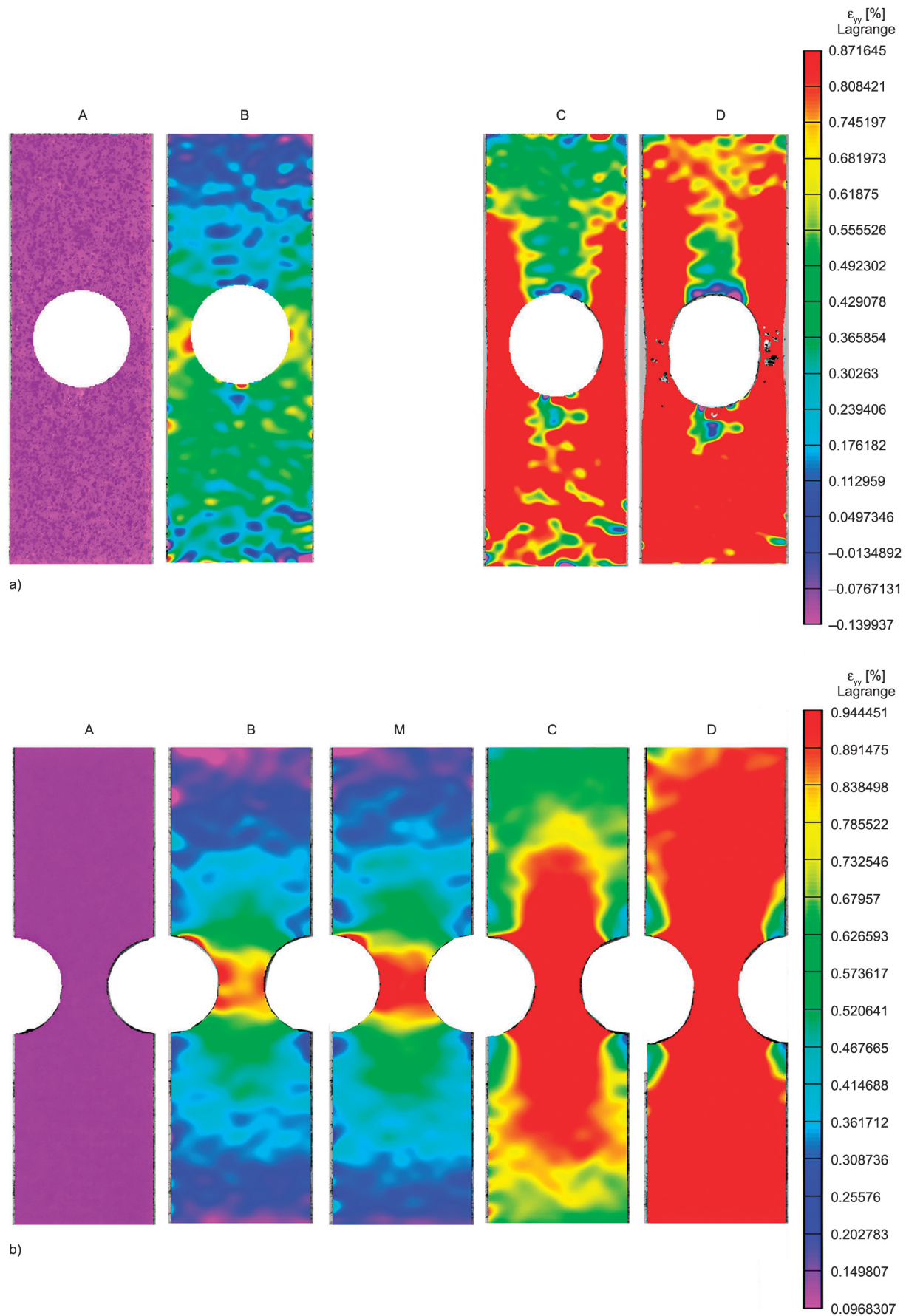


**Figure 6.** Colorized contour of srPETs at  $W/D$  ratio = 1.5. (a) Points B, C, and D for CH specimens. (b) Points B, M, C, and D for DESH specimens.



**Table 2.** Value of  $\epsilon_{\text{hole}}$ ,  $\epsilon_{\text{avg}}$ , and  $\epsilon_{\text{end}}$  at points B, C, and D in the CH srPETs, and the  $\epsilon_{\text{hole}}$ ,  $\epsilon_{\text{middle}}$ ,  $\epsilon_{\text{avg}}$ , and  $\epsilon_{\text{end}}$  at points B, M, C, and D in the DESH srPETs.

	B		M	C		D	
	DESH	CH	DESH	DESH	CH	DESH	CH
	<i>W/D</i> = 3.5						
$\epsilon_{\text{hole}}$ [%]	<b>1.42±0.02</b>	<b>1.33±0.02</b>	3.20±0.03	5.01±0.06	5.7±0.04	10.34±0.07	12.44±0.05
$\epsilon_{\text{middle}}$ [%]	0.75±0.03		<b>1.40±0.03</b>	2.01±0.05		4.27±0.04	
$\epsilon_{\text{avg}}$ [%]	0.65±0.01	0.52±0.02	1.11±0.02	<b>1.41±0.03</b>	<b>1.32±0.02</b>	2.27±0.03	2.23±0.02
$\epsilon_{\text{end}}$ [%]	0.51±0.04	0.46±0.01	0.98±0.03	1.21±0.05	1.10±0.04	<b>1.41±0.03</b>	<b>1.34±0.02</b>
	<i>W/D</i> = 1.5						
	$\epsilon_{\text{hole}}$ [%]	<b>0.93±0.02</b>	<b>0.85±0.03</b>	1.09±0.04	2.61±0.05	3.10±0.06	16.40±0.12
	$\epsilon_{\text{middle}}$ [%]	0.84±0.03		<b>0.93±0.03</b>	2.59±0.06		13.50±0.11
	$\epsilon_{\text{avg}}$ [%]	0.47±0.03	0.42±0.03	0.53±0.04	<b>0.94±0.02</b>	<b>0.86±0.03</b>	2.12±0.04
	$\epsilon_{\text{end}}$ [%]	0.25±0.02	0.27±0.01	0.31±0.03	0.75±0.03	0.64±0.04	<b>0.94±0.02</b>

and D. Further, as shown in Figure 4a, the strain value of point E is higher than that of CH. *W/D* ratio = 2.5 follows a similar trend to *W/D* ratio = 3.5; however, with lower  $K_{\epsilon}$  values throughout the deformation. Similarly, srPET with DESH shows a relatively lower  $K_{\epsilon}$  than CH because of strain coupling.

Figure 4b shows the change in  $K_{\epsilon}$  at *W/D* ratio = 1.5. At point B, the strain at the edge of the hole is equal to  $\epsilon_y$  (Table 2), which implies that local yielding has occurred. After point B, the yield extends from the edge of the hole, where plastic deformation occurs. In addition, the  $K_{\epsilon}$  increment at point M (Figure 4b of srPET with DESH) is relatively lower than that at other *W/D* ratios because point M approaches point B with a decrease in the *W/D* ratio; then, the  $K_{\epsilon}$  of srPETs increases rapidly.

The plastic deformation after point C caused the propagation of the yield extent. However, the spread of the yield extent was relatively slow because of the smaller ligaments, and this resulted in a very high  $K_{\epsilon}$  at point D ( $K_{\epsilon}$  = 9.52 and 7.85 for srPETs with CH and with DESH, respectively). However, CH had a higher  $K_{\epsilon}$  and  $\epsilon_{\text{hole}}$  (23.29%, as listed in Table 2) than DESH. Thus, the ligament of the CH specimen was unable to support any further load, and therefore, the  $K_{\epsilon}$  curve did not decrease significantly (as indicated in Figure 4b). Thus, this unusually high  $K_{\epsilon}$  at point D at *W/D* ratio = 1.5 can invalidate the results for  $K_{\sigma}$  estimation. srPET with *W/D* ratio  $\leq 1.5$  is not recommended as a parameter for structural part design.

### 3.4. Stress concentration factor of srPETs with CH and DESH

The  $K_{\sigma}$  values of srPET with CH and DESH are obtained by DIC using Neuber's rule [53] is shown in

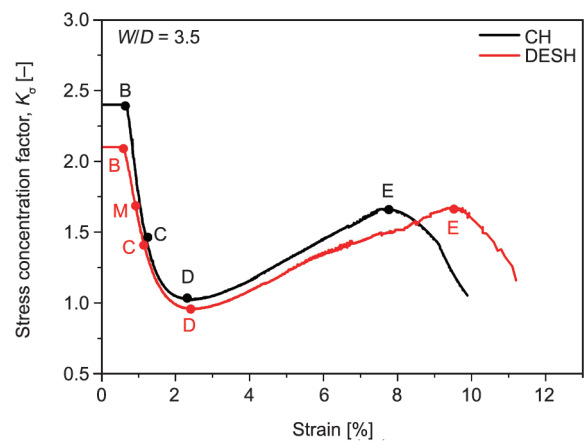
**Figure 7.** Stress concentration factor ( $K_{\sigma}$ ) of the srPETs with CH and DESH measured using the DIC method at *W/D* ratio = 3.5.

Figure 7. The  $K_{\sigma}$  curve is the inverse of  $K_{\epsilon}$ , and it follows all stages of the  $K_{\epsilon}$  curve. The srPETs with DESH were lower than those with CH, which resulted in higher tensile strength and strain. Figure 7 shows that  $K_{\sigma}$  is equal to  $K_t$  before point B. After point B, the  $K_{\sigma}$  curves for the DESH and CH specimens began to decrease; after point M, DESH decreases more than CH because of strain coupling. Further, after point D,  $K_{\sigma}$  starts to increase to the crack initiation point (point E); this is triggered by the large deformations and results in a significant change in the hole shape. The shape changed from a circle to an ellipse because the hole deformed in the direction of the force (Figure 3). At point E, the  $K_{\sigma}$  value is lower than that of PMMA; however, the strain at the edge of the hole is close to the failure strain of the srPET (24%). This leads to failure after crack initiation at point E. The results at *W/D* ratio = 2.5 followed a similar trend as those for *W/D* ratio = 3.5; however, with lower values of  $K_{\sigma}$ .

### 3.5. Dissipation of strain concentration factors versus $a/r$ for srPETs with CH and DESH

The  $K_\varepsilon$  dissipation for the  $a/r$  of PMMA with CH and DESH at different strains (30, 60, and 90%) was obtained. The dissipation of  $K_\varepsilon$  was independent of strain because of the linear elastic response of PMMA. Figure 8 shows the dissipation of  $K_\varepsilon$  relative to  $a/r$  at points B, C, and D under different  $W/D$  ratios for

srPET (CH and DESH). Unlike the PMMA materials, the dissipation of  $K_\varepsilon$  was different at different stages (B, C, and D); however, the  $K_\varepsilon$  dissipation at point B of srPETs was the same as that of the PMMA at the same  $W/D$  ratio.

Figure 8a shows that, for srPET with CH and  $W/D$  ratio = 3.5, the dissipation of  $K_\varepsilon$  is steep with an increasing distance from the hole edge ( $a/r = 1$ ) and it

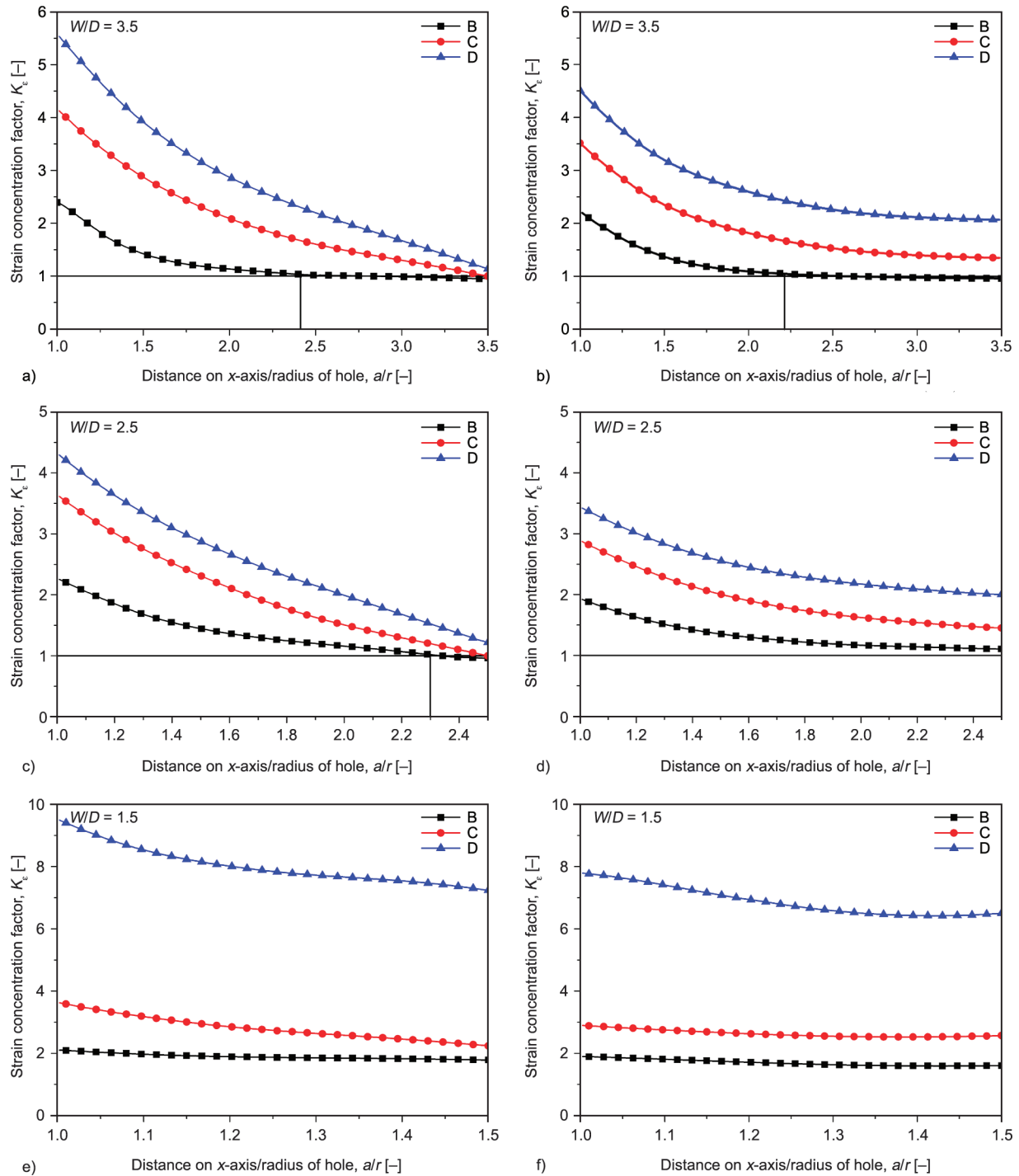


**Figure 8.** Dissipation of  $K_\varepsilon$  of srPETs with distance on x-axis/radius of hole ( $a/r$ ) = 1 to 3.5, 2.5 and 1.5 for  $W/D$  ratios = 3.5, 2.5 and 1.5 respectively, at points B, C, and D. (a), (c), and (e) for CH specimens. (b), (d), and (f) for DESH specimens.

is completely dissipated at  $a/r = 2.4$ . In addition, Figure 8b shows that the dissipation of  $K_e$  is more gradual than that of CH, and it completely dissipates at  $a/r = 2.2$  for srPETs with DESH. The results indicate that strain coupling in the DESH results in a smaller affected area of the SC at the hole edge.  $K_e$  is completely dissipated at the sample edge ( $a/r = 3.5$ ) when srPET with CH undergoes plastic deformation (points C and D); however, for DESH,  $K_e$  is not completely dissipated because of the strain coupling effects. For  $W/D$  ratio = 2.5 (Figure 8c), the  $K_e$  dissipation follow a similar trend as that for  $W/D$  ratio = 3.5. The  $K_e$  dissipation in srPET with CH at point B is relatively less than that at  $W/D$  ratio = 3.5, and it completely dissipates at  $a/r = 2.3$ , whereas the dissipation in DESH is more moderate (Figure 8d). At point D in srPET with CH,  $K_e$  did not completely dissipate at the sample edge, unlike that at  $W/D$  ratio = 3.5.

Figures 8e and 8f show the dissipation of  $K_e$  at points B, C, and D of srPETs at  $W/D$  ratio = 1.5. At point B, a straight  $K_e$  curve was obtained and was independent of  $a/r$ ; that is, the ligament was not sufficiently wide to dissipate the concentrated strain energy. Further, at point C, a straight  $K_e$  curve was obtained for srPET with DESH, whereas a slight dissipation was observed for CH; this can be attributed to the strain coupling effect. At point D, although slight dissipation was observed in srPET, its  $K_e$  remained at a very high value throughout the ligament, *i.e.*, its strain value was close to the material failure strain of 23%. Thus, this unexpected increase in  $K_e$  suggests that srPET with  $W/D$  ratio  $\leq 1.5$  is not recommended as a parameter for structural part design.

#### 4. Conclusions

- In this study, the variation in  $K_e$  within the full deformation range of srPETs DESH using DIC at different  $W/D$  ratios was investigated for the first time, to the best of the author's knowledge. The  $K_e$  curve was divided into six stages based on the spread of the yield extent.  $K_e$  started from the theoretical concentration factor ( $K_t$ ) within the elastic deformation, and then rapidly increased to a peak value at which point the entire sample reached yield; then, it fell to a minimum value, which was an early warning point for material failure.
- At  $W/D$  ratio = 2.5, the strength retention of srPET was 87% for CH and 95% for DESH; this was

better than that for brittle composites because of the super ductile behavior of srPETs.

- $K_e$  decreased in the elastic and plastic deformation regions with a decrease in the  $W/D$  ratio. The  $K_e$  value of srPET with DESH was lower than that of the srPET with the CH because of strain coupling. Thus, the DESH samples exhibited better tensile properties than the CH samples.
- The dissipation of  $K_e$  was independent of the strain because of the linear elastic response of the PMMA material. The dissipation of the  $K_e$  of the srPETs differed at different stages (B, C, and D).  $K_e$  was completely dissipated at the sample edge ( $a/r = 3.5$ ) when srPET with CH underwent plastic deformation (points C and D); for DESH,  $K_e$  was not completely dissipated because of the strain coupling effects.
- The decrease in  $K_e$  after local yielding near the edge of the hole prolongs the load-carrying capacity of ductile materials such as srPET composites. For the safe structural design of ductile composites such as srPET composites,  $W/D > 1.5$  is recommended. The research results help to understand the progress of yield deformation caused by strain/stress concentration near the hole edge and its final failure in ductile materials such as srPET composites, and provide an important reference for the geometric design of hole drilling structural parts in practical applications.

#### Acknowledgements

This work is partially supported by the Ministry of Science and Technology of Taiwan, R.O.C. under grant numbers: MOST 110-2811-E-011 -505 -MY3.

#### References

- [1] May D., Goergen C., Friedrich K.: Multifunctionality of polymer composites based on recycled carbon fibers: A review. *Advanced Industrial and Engineering Polymer Research*, **4**, 70–81 (2021).  
<https://doi.org/10.1016/j.aiepr.2021.01.001>
- [2] Job S.: Recycling composites commercially. *Reinforced Plastics*, **58**, 32–38 (2014).  
[https://doi.org/10.1016/S0034-3617\(14\)70213-9](https://doi.org/10.1016/S0034-3617(14)70213-9)
- [3] Yang Y., Boom R., Irion B., van Heerden D-J., Kuiper P., de Wit H.: Recycling of composite materials. *Chemical Engineering and Processing-Process Intensification*, **51**, 53–68 (2012).  
<https://doi.org/10.1016/j.cep.2011.09.007>

- [4] López F. A., Rodríguez O., Alguacil F. J., García-Díaz I., Centeno T. A., García-Fierro J. L., González C.: Recovery of carbon fibres by the thermolysis and gasification of waste prepreg. *Journal of Analytical and Applied Pyrolysis*, **104**, 675–683 (2013).  
<https://doi.org/10.1016/j.jaap.2013.04.012>
- [5] Ma S., Webster D. C.: Degradable thermosets based on labile bonds or linkages: A review. *Progress in Polymer Science*, **76**, 65–110 (2018).  
<https://doi.org/10.1016/j.progpolymsci.2017.07.008>
- [6] Asmatulu E., Twomey J., Overcash M.: Recycling of fiber-reinforced composites and direct structural composite recycling concept. *Journal of Composite Materials*, **48**, 593–608 (2014).  
<https://doi.org/10.1177/0021998313476325>
- [7] Utekar S., Suriya V. K., More N., Rao A.: Comprehensive study of recycling of thermosetting polymer composites – Driving force, challenges and methods. *Composites Part B: Engineering*, **207**, 108596 (2021).  
<https://doi.org/10.1016/j.compositesb.2020.108596>
- [8] Fakirov S.: Nano-/microfibrillar polymer-polymer and single polymer composites: The converting instead of adding concept. *Composites Science and Technology*, **89**, 211–225 (2013).  
<https://doi.org/10.1016/j.compscitech.2013.10.007>
- [9] Dorigato A., Fredi G., Fambri L., Lopez-Cuesta J-M., Pegoretti A.: Polyethylene-based single polymer laminates: Synergistic effects of nanosilica and metal hydroxides. *Journal of Reinforced Plastics and Composites*, **38**, 62–73 (2019).  
<https://doi.org/10.1177/0731684418802974>
- [10] Kmetty Á., Bárány T., Karger-Kocsis J.: Self-reinforced polymeric materials: A review. *Progress in Polymer Science*, **35**, 1288–1310 (2010).  
<https://doi.org/10.1016/j.progpolymsci.2010.07.002>
- [11] Karger-Kocsis J., Bárány T.: Single-polymer composites (SPCs): Status and future trends. *Composites Science and Technology*, **92**, 77–94 (2014).  
<https://doi.org/10.1016/j.compscitech.2013.12.006>
- [12] Zhang J. M., Peijs T.: Self-reinforced poly(ethylene terephthalate) composites by hot consolidation of bi-component PET yarns. *Composites Part A: Applied Science and Manufacturing*, **41**, 964–972 (2010).  
<https://doi.org/10.1016/j.compositesa.2010.03.012>
- [13] Zhang J. M., Reynolds C. T., Peijs T.: All-poly(ethylene terephthalate) composites by film stacking of oriented tapes. *Composites Part A: Applied Science and Manufacturing*, **40**, 1747–1755 (2009).  
<https://doi.org/10.1016/j.compositesa.2009.08.008>
- [14] Abraham T. N., Wanjale S. D., Bárány T., Karger-Kocsis J.: Tensile mechanical and perforation impact behavior of all-PP composites containing random PP copolymer as matrix and stretched PP homopolymer as reinforcement: Effect of  $\beta$  nucleation of the matrix. *Composites Part A: Applied Science and Manufacturing*, **40**, 662–668 (2009).  
<https://doi.org/10.1016/j.compositesa.2009.03.001>
- [15] Romhány G., Wu C. M., Lai W. Y., Karger-Kocsis J.: Fracture behavior and damage development in self-reinforced PET composites assessed by located acoustic emission and thermography: Effects of flame retardant and recycled PET. *Composites Science and Technology*, **132**, 76–83 (2016).  
<https://doi.org/10.1016/j.compscitech.2016.06.014>
- [16] Wu C-M., Lin P-C., Kumar S., Chen J-C.: Long-term open-hole tensile creep properties of self-reinforced PET composites measured by digital image correlation. *Materials Chemistry and Physics*, **278**, 125633 (2022).  
<https://doi.org/10.1016/j.matchemphys.2021.125633>
- [17] Kumar S., Wu C-M., Lai W-Y., Lin P-C.: Pin hole tensile and fatigue properties of self-reinforced PET composites. *Composite Structures*, **255**, 112981 (2021).  
<https://doi.org/10.1016/j.compstruct.2020.112981>
- [18] Wu C. M., Lin P. C., Murakami R.: Long-term creep behavior of self-reinforced PET composites. *Express Polymer Letters*, **11**, 820–831 (2017).  
<https://doi.org/10.3144/expresspolymlett.2017.78>
- [19] Wu C-M., Lai W-Y.: Mechanical and open hole tensile properties of self-reinforced PET composites with recycled PET fiber reinforcement. *Journal of Applied Polymer Science*, **133**, 43682 (2016).  
<https://doi.org/10.1002/app.43682>
- [20] Roark R., Sadegh A.: Roark's formulas for stress and strain. McGraw-Hill, New York Chicago (1989).
- [21] Zhou Y., Lin Q., Hong J., Yang N.: Optimal design of functionally graded material for stress concentration reduction. *Structures*, **29**, 561–569 (2021).  
<https://doi.org/10.1016/j.istruc.2020.11.053>
- [22] Zhao J., Zhou H., Sun X., Jing Y.: Evaluation on compressive properties of composite laminates with a hole reinforced by metal plate. *Composite Structures*, **258**, 113423 (2021).  
<https://doi.org/10.1016/j.compstruct.2020.113423>
- [23] Zheng C., Li X., Mi C.: Reducing stress concentrations in unidirectionally tensioned thick-walled spheres through embedding a functionally graded reinforcement. *International Journal of Mechanical Sciences*, **152**, 257–267 (2019).  
<https://doi.org/10.1016/j.ijmecsci.2018.12.055>
- [24] Zheng M., Yin Z., Teng H., Liu J., Wang Y.: Elastoplastic behavior of highly ductile materials. Springer Nature, Singapore (2019).  
<https://doi.org/10.1007/978-981-15-0906-3>
- [25] Shi S-Q., Puls M. P.: A simple method of estimating the maximum normal stress and plastic zone size at a shallow notch. *International Journal of Pressure Vessels and Piping*, **64**, 67–71 (1995).  
[https://doi.org/10.1016/0308-0161\(94\)00070-Y](https://doi.org/10.1016/0308-0161(94)00070-Y)
- [26] Polák J.: Stress and strain concentration factor evaluation using the equivalent energy concept. *Materials Science and Engineering*, **61**, 195–200 (1983).  
[https://doi.org/10.1016/0025-5416\(83\)90100-3](https://doi.org/10.1016/0025-5416(83)90100-3)



- [27] Molski K., Glinka G.: A method of elastic-plastic stress and strain calculation at a notch root. *Materials Science and Engineering*, **50**, 93–100 (1981).  
[https://doi.org/10.1016/0025-5416\(81\)90089-6](https://doi.org/10.1016/0025-5416(81)90089-6)
- [28] Romanowicz P. J., Szybiński B., Wygoda M.: Application of DIC method in the analysis of stress concentration and plastic zone development problems. *Materials*, **13**, 3460 (2020).  
<https://doi.org/10.3390/ma13163460>
- [29] Murakami Y.: *Theory of elasticity and stress concentration*. Wiley, London (2017).
- [30] Providakis C. P., Sotiropoulos D. A.: A BEM approach to the stress concentration reduction in visco-plastic plates by multiple holes. *Computers and Structures*, **64**, 313–317 (1997).  
[https://doi.org/10.1016/S0045-7949\(96\)00152-6](https://doi.org/10.1016/S0045-7949(96)00152-6)
- [31] Khoshhravan M. R., Samaei M., Paykani A.: Numerical investigation on the position of holes for reducing stress concentration in composite plates with bolted and riveted joints. *Theoretical and Applied Mechanics Letters*, **1**, 041005 (2011).  
<https://doi.org/10.1063/2.1104105>
- [32] Meguid S. A.: Finite element analysis of defence hole systems for the reduction of stress concentration in a uniaxially-loaded plate with two coaxial holes. *Engineering Fracture Mechanics*, **25**, 403–413 (1986).  
[https://doi.org/10.1016/0013-7944\(86\)90254-7](https://doi.org/10.1016/0013-7944(86)90254-7)
- [33] Özaslan E., Güler M. A., Yetgin A., Acar B.: Stress analysis and strength prediction of composite laminates with two interacting holes. *Composite Structures*, **221**, 110869 (2019).  
<https://doi.org/10.1016/j.compstruct.2019.04.041>
- [34] Nagpal S., Jain N., Sanyal S.: Stress concentration and its mitigation techniques in flat plate with singularities-A critical review. *Engineering Journal*, **16**, 1–16 (2012).  
<https://doi.org/10.4186/ej.2012.16.1.1>
- [35] Sun J., Jing Z., Wu J., Wang W., Zhang D., Zhao J.: Strain rate effects on dynamic tensile properties of open-hole composite laminates. *Composites Communications*, **19**, 226–232 (2020).  
<https://doi.org/10.1016/j.coco.2020.04.004>
- [36] Barrowman E. M.: High-elongation strain measurement. *Experimental Techniques*, **7**, 29–32 (1982).  
<https://doi.org/10.1111/j.1747-1567.1983.tb01681.x>
- [37] Malezhik M. P., Malezhik O. P., Zirka A. I., Chernyshenko I. S.: Dynamic photoelastic study of wave fields in elastic plates with stress concentrators. *International Applied Mechanics*, **41**, 1399–1406 (2005).  
<https://doi.org/10.1007/s10778-006-0048-5>
- [38] Rubayi N. A., Nana A. D.: Photoelastic stress analysis of an elliptical hole in a thick plate subjected to uniform in-plane compressive loading. *Experimental Mechanics*, **25**, 105–114 (1985).  
<https://doi.org/10.1007/BF02328799>
- [39] Meguid S. A., Tan M. A.: Photoelastic analysis of the singular stress field in a bimaterial wedge. *Experimental Mechanics*, **40**, 68–74 (2000).  
<https://doi.org/10.1007/BF02327550>
- [40] Suh J-G., Hawong J-S., Shin D-C.: A study of the development of the stress optic law of photoelastic experiment considering residual stress. *KSME International Journal*, **17**, 1674–1681 (2003).  
<https://doi.org/10.1007/BF02983597>
- [41] Woolard D. F.: *Thermoelastic and photoelastic full-field stress measurement*. College of William and Mary, PhD Thesis (1999).  
<https://doi.org/10.21220/s2-x5mm-jq08>
- [42] Szebényi G., Hliva V.: Detection of delamination in polymer composites by digital image correlation-experimental test. *Polymers*, **11**, 523 (2019).  
<https://doi.org/10.3390/polym11030523>
- [43] Wu C-M., Kumar S., Lin P-C., Chen J-C.: Strain and stress concentration of ductile composites in full-range deformation by digital image correlation. *Mechanics of Advanced Materials and Structures*, in press (2022).  
<https://doi.org/10.1080/15376494.2022.2084192>
- [44] O'Higgins R. M., McCarthy M. A., McCarthy C. T.: Comparison of open hole tension characteristics of high strength glass and carbon fibre-reinforced composite materials. *Composites Science and Technology*, **68**, 2770–2778 (2008).  
<https://doi.org/10.1016/j.compscitech.2008.06.003>
- [45] Yudhanto A., Watanabe N., Iwahori Y., Hoshi H.: The effects of stitch orientation on the tensile and open hole tension properties of carbon/epoxy plain weave laminates. *Materials and Design*, **35**, 563–571 (2012).  
<https://doi.org/10.1016/j.matdes.2011.09.013>
- [46] Vieille B., Aucher J., Taleb L.: Comparative study on the behavior of woven-ply reinforced thermoplastic or thermosetting laminates under severe environmental conditions. *Materials and Design*, **35**, 707–719 (2012).  
<https://doi.org/10.1016/j.matdes.2011.10.037>
- [47] Zhang Y., Guo Q., Chen X., Xie J., Chen L.: Effect of apertures on tensile property of warp-reinforced 2.5D woven composites notched plates. *Composite Structures*, **252**, 112693 (2020).  
<https://doi.org/10.1016/j.compstruct.2020.112693>
- [48] Hao A., Yuan L., Chen J. Y.: Notch effects and crack propagation analysis on kenaf/polypropylene nonwoven composites. *Composites Part A: Applied Science and Manufacturing*, **73**, 11–19 (2015).  
<https://doi.org/10.1016/j.compositesa.2015.02.016>
- [49] Gobi Kannan T., Wu C. M., Cheng K. B.: Influence of laminate lay-up, hole size and coupling agent on the open hole tensile properties of flax yarn reinforced polypropylene laminates. *Composites Part B: Engineering*, **57**, 80–85 (2014).  
<https://doi.org/10.1016/j.compositesb.2013.09.042>
- [50] Nijs A., Selezneva M., Swolfs Y., Hirano N., Taketa I., Karki T., Verpoest I., Gorbatiikh L.: Notch-sensitivity of hybrid carbon-fibre/self-reinforced polypropylene composites. *Composites Science and Technology*, **200**, 108422 (2020).  
<https://doi.org/10.1016/j.compscitech.2020.108422>

- [51] Khechai A., Tati A., Guerira B., Guettala A., Mohite P. M.: Strength degradation and stress analysis of composite plates with circular, square and rectangular notches using digital image correlation. *Composite Structures*, **185**, 699–715 (2018).  
<https://doi.org/10.1016/j.compstruct.2017.11.060>
- [52] Peterson R. E.: *Stress concentration design factors : Charts and relations useful in making strength calculations for machine parts and structural elements*. Wiley, New York (1974).
- [53] Makhutov N. A., Reznikov D. O.: Generalization of Neuber's rule for the assessment of local stresses and strains in stress concentration zones for a wide range of applied strains. *Procedia Structural Integrity*, **14**, 199–206 (2019).  
<https://doi.org/10.1016/j.prostr.2019.05.026>